Behavioral/Cognitive

Multisession Anodal Transcranial Direct Current Stimulation Enhances Adult Hippocampal Neurogenesis and Context Discrimination in Mice

Ting-Hsuan Yu,[1] Yi-Jen Wu,[2,3] Miao-Er Chien,[2,3] and Kuei-Sen Hsu[1,4]

[1]Institute of Basic Medical Sciences, College of Medicine, National Cheng Kung University, Tainan 70101, Taiwan, [2]Department of Neurology, National Cheng Kung University Hospital, College of Medicine, National Cheng Kung University, Tainan 70457, Taiwan, [3]Institute of Clinical Medicine, College of Medicine, National Cheng Kung University, Tainan 70457, Taiwan, and [4]Department of Pharmacology, College of Medicine, National Cheng Kung University, Tainan 70101, Taiwan

Transcranial direct current stimulation (tDCS) is a promising noninvasive neuromodulatory treatment option for multiple neurologic and psychiatric disorders, but its mechanism of action is still poorly understood. Adult hippocampal neurogenesis (AHN) continues throughout life and is crucial for preserving several aspects of hippocampal-dependent cognitive functions. Nevertheless, the contribution of AHN in the neuromodulatory effects of tDCS remains unexplored. Here, we sought to investigate whether multisession anodal tDCS may modulate AHN and its associated cognitive functions. Multisession anodal tDCS were applied on the skull over the hippocampus of adult male mice for 20 min at 0.25 mA once daily for 10 d totally. We found that multisession anodal tDCS enhances AHN by increasing the proliferation, differentiation and survival of neural stem/progenitor cells (NSPCs). In addition, tDCS treatment increased cell cycle reentry and reduced cell cycle exit of NSPCs. The tDCS-treated mice exhibited a reduced GABAergic inhibitory tone in the dentate gyrus compared with sham-treated mice. The effect of tDCS on the proliferation of NSPCs was blocked by pharmacological restoration of $GABA_B$ receptor-mediated inhibition. Functionally, multisession anodal tDCS enhances performance on a contextual fear discrimination task, and this enhancement was prevented by blocking AHN using the DNA alkylating agent temozolomide (TMZ). Our results emphasize an important role for AHN in mediating the beneficial effects of tDCS on cognitive functions that substantially broadens the mechanistic understanding of tDCS beyond its well-described in hippocampal synaptic plasticity.

Key words: **adult neurogenesis; context discrimination; GABAergic inhibition; hippocampus; neural stem/progenitor cells; transcranial direct current stimulation**

Significance Statement

Transcranial direct current stimulation (tDCS) has been shown to effectively enhance cognitive functions in healthy and pathologic conditions. However, the mechanisms underlying its effects are largely unknown and need to be better understood to enable its optimal clinical use. This study shows that multisession anodal tDCS enhances adult hippocampal neurogenesis (AHN) and therefore contributes to enhance context discrimination in mice. Our results also show that the effect of tDCS on AHN is associated with reduced GABAergic inhibition in the dentate gyrus. Our study uncovers a novel mechanism of anodal tDCS to elicit cognitive-enhancing effects and may have the potential to improve cognitive decline associated with normal aging and neurodegenerative disorders.

Received Aug. 2, 2022; revised Nov. 27, 2022; accepted Dec. 4, 2022.

Author contributions: K.-S.H., T.-H.Y., Y.-J.W., and M.-E.C. designed research; T.-H.Y. and M.-E.C. performed research; T.-H.Y. and M.-E.C. analyzed data; K.-S.H. and T.-H.Y. wrote the first draft of the paper; K.-S.H., T.-H.Y., Y.-J.W., and M.-E.C. edited the paper; K.-S.H., T.-H.Y., and Y.-J.W. wrote the paper.

This work was supported by the National Health Research Institute Research Grant NHRI-EX110-10912NI and by Ministry of Science and Technology Research Grants 106-2320-B-006-026-MY3, 107-2320-B-006-037-MY3, 108-2331-B-006-025-MY2, and 109-2320-B-006-039-MY3 of Taiwan. We thank members of the Hsu's Lab for valuable discussions and suggestions.

The authors declare no competing financial interests.

Correspondence should be addressed to Kuei-Sen Hsu at richard@mail.ncku.edu.tw.

https://doi.org/10.1523/JNEUROSCI.1476-22.2022

Introduction

Transcranial direct current stimulation (tDCS) is a noninvasive brain stimulation technique that involves the application of a constant low-intensity electrical current through epicranial electrodes positioned over the brain regions of interest (Brunoni et al., 2012; Chan et al., 2021). The promising clinical outcomes obtained across multiple disease conditions coupled with the fact that this approach is generally safe, well-tolerated, inexpensive and simple to administer have catalyzed the popularity of tDCS and its potential use in clinical practice (Pelletier and Cicchetti,

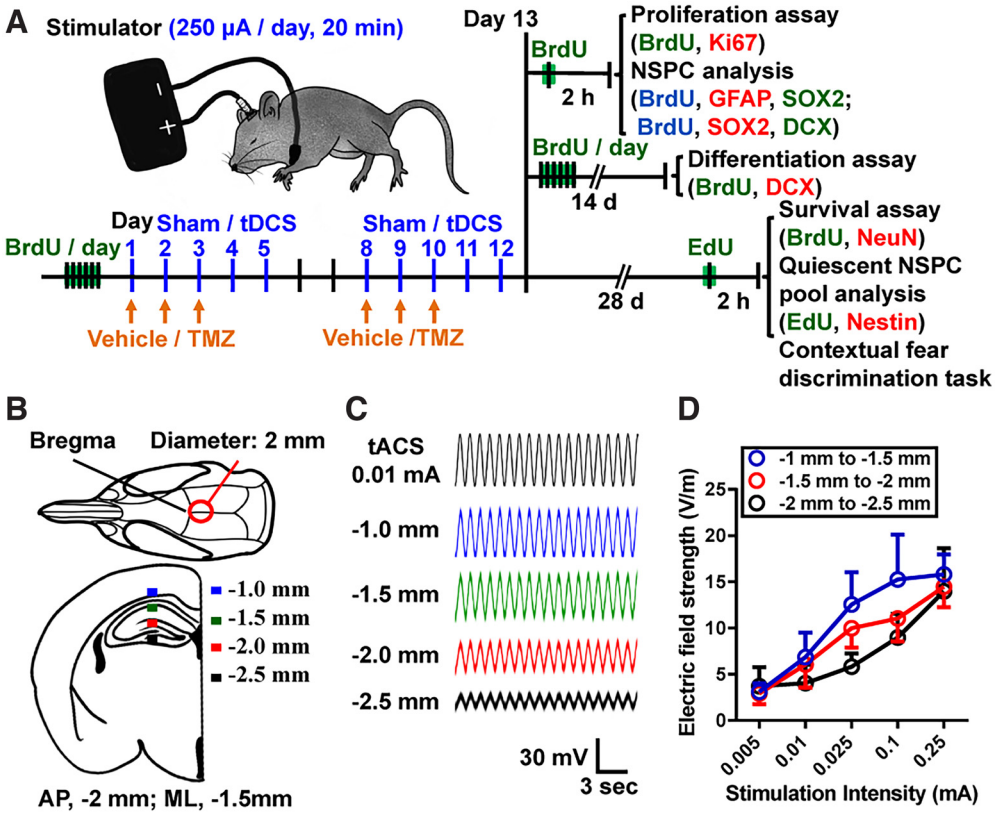

Figure 1. Illustration of tDCS stimulation in mice and experimental designs. ***A***, Multisession anodal sham (250 μA, 10 s) or tDCS (250 μA, 20 min) stimulation repeated daily for five consecutive days, followed by a sham-free or tDCS-free interval of 2 d, then mice were subjected to sham or tDCS for five more days, for a total of 10 d. For proliferation assay and NSPC population analysis, mice received a single BrdU (50 mg/kg) injection 1 d after last sham or tDCS application and were killed 2 h after BrdU injection for immunolabelling, imaging, and analysis. For quantification of neuronal differentiation, mice were injected six times intraperitoneally with BrdU at 12-h intervals and killed by transcardial perfusion after 14 d after the last BrdU injection. For quantification of neuronal survival, mice were injected six times intraperitoneally with BrdU at 12-h intervals before tDCS application and killed by transcardial perfusion after 40 d after the last BrdU injection. For quiescent NSPC pool quantification, mice were received a single EdU (50 mg/kg) injection 28 d after last tDCS application and mice were killed 2 h after EdU injection for immunolabelling, imaging, and analysis. Contextual fear discrimination learning task was started 28 d after sham or tDCS application. ***B***, Schematic representation of electric fields recorded in the dorsal hippocampus at different depths. ***C***, tACS stimulation applied over the scalp and sampling trace of the actual potentials generated at different depth. ***D***, Mean electric fields recorded at different depths for tACS application (two-way repeated measure ANOVA, Intensity: $F_{(4,20)} = 14.11$, $p < 0.0001$; Depth: $F_{(2,10)} = 18.94$, $p = 0.0004$; Interaction: $F_{(8,40)} = 0.72$ $p = 0.6722$; $n = 6$ in each group). Data are presented as mean ± SEM.

2014). To date, tDCS has already demonstrated its abilities to improve motor deficits caused by stroke or Parkinson's disease, and cognitive abilities in patients suffering from neuropsychiatric disorders such as schizophrenia, epilepsy, depression, mild cognitive impairment, and Alzheimer's disease (Fregni et al., 2006; Ferrucci et al., 2008; Göder et al., 2013; Flöel, 2014). Despite these beneficial effects found in patients, tDCS has reliably been shown to enhance declarative and working memory capacity in healthy individuals (Fregni et al., 2005; Wu et al., 2014). However, the mechanisms underlying its effects are largely unknown and needs to be better understood to enable its optimal clinical use.

tDCS effects are often attributed to the modulation of neuronal activity of superficial cortical layers; however, deep brain structures may also be affected because of the physicals of current flow through the brain to the reference electrode. Accordingly, both preclinical and clinical studies have shown that the hippocampus is one of the brain regions vulnerable to the effects of tDCS. For example, in older subjects, anodal tDCS over the left temporoparietal cortex accelerates learning and improves retrieval of newly acquired episodic memory by tuning hippocampal-temporoparietal functional networks (Antonenko et al., 2019). In rodents, we and others have recently shown that anodal tDCS facilitates the induction of long-term potentiation (LTP) at Schaffer collateral-CA1 synapses and enhances memory performance in hippocampal-dependent passive avoidance learning task (Yu et al., 2019; Farahani et al., 2021). There is also evidence that bilateral tDCS over the temporal lobes decreases pattern separation in healthy young adults (Cappiello et al., 2016). Despite being associated with memory encoding and mood regulation, adult neurogenesis in the dentate gyrus (DG) of the hippocampus is causally involved in behavioral pattern separation (Clelland et al., 2009; Sahay et al., 2011). However, it is not yet clear whether tDCS may affect adult hippocampal neurogenesis (AHN), thus modulating pattern separation. Because multiple sessions of tDCS allows cumulative effects and is more efficacious than a single session (Pedron et al., 2014; Alizadehgoradel et al., 2020), we decided to target AHN with a multisession anodal tDCS protocol. We first explored the impact of tDCS on different stages of AHN using 5-bromo-2'-deoxyuridine (BrdU) labeling and immunofluorescence staining approaches. We then assessed the role of tDCS-induced changes in AHN in cognitive function using a contextual fear discrimination task that is commonly used to study memory interference (Miller and Sahay, 2019). We demonstrate for the first time in an animal model that multisession anodal tDCS can effectively enhance AHN and then promote context discrimination. This study also uncovers a novel mechanism underlying the putative cognitive-enhancing effects of anodal tDCS.

Materials and Methods

Animals

Eight- to 12-week-old male C57BL/6J mice were used. Mice were housed five per cage under a 12/12 h light/dark cycle and were randomized to receive sham or tDCS stimulation. All experimental procedures were conducted in accordance with the National Institutes of Health *Guidelines for the Care and Use of Laboratory Animals* and were approved by the Institutional Animal Care and Use Committee of National Cheng Kung University (authorization approval no. 110282). The exclusion of female mice from studies because of estrous cycle variability may increase variance relative to males. All efforts were made to minimize animal suffering and to use only the numbers of animals necessary to produce reliable scientific data. The investigators were kept blind to the group allocation while performing behavioral ratings and quantification of immunofluorescence.

Cranial electrode implantation and tDCS treatment

Mice were anesthetized with a mixture of 50- to 60-mg/kg zolazepam (Zoletil, Virbac) and 5.8- to 6.5-mg/kg xylazine hydrochloride (Rompun, Bayer) during surgery. A 2.0 mm (internal diameter) tubular plastic cannula was placed on the skull with the center of the electrode resting on the midline and 1 mm caudal to bregma. The tubular plastic cannula was fixed with dental cement (Lang Dental Manufacturing Co Inc.). One week after surgery, the plastic tube was filled with saline solution (0.9% NaCl), a silver-coated tDCS electrode (A-M Systems) was inserted, and a surface reference electrode (0.25 cm^2, Ambu A/S) was placed under the shaved thorax as counter electrode. Anodal tDCS was applied continuously for 20 min using a constant current stimulator (DC-Stimulator Plus, NeuroConn). For lowering anxiety and stress, mice were lightly anesthetized with low doses of zolazepam (10 mg/kg) and xylazine hydrochloride (1 mg/kg) during anodal tDCS (250 μA/3.14 mm^2, 20 min) and sham (250 μA/3.14 mm^2, 10 s) stimulation. tDCS was repeated daily for five consecutive days, followed by a tDCS-free interval of 2 d, then mice were subjected to tDCS for five more days, for a total of 10 d. The stimulation protocol was chosen on the basis of the previous studies (Braun et al., 2016; Pikhovych et al., 2016) with minor modification. After each stimulation session, mice were returned to their homecage and had access to food and water *ad libitum*.

Transcranial alternating current stimulation (tACS)-induced intracranial electric fields recording

To measure the actual electric field elicited intracranially, tACS was generated at five intensities (0.001 mA, 0.025 mA, 0.05 mA, 0.1 mA, and 0.25 mA) with 1 Hz by Linear isolated stimulator (BIOPAC System). Four hand-made stainless electrodes (50.8 mm diameter coated with polymin, California Fine Wire Company) were placed in different depth (1–2.5 mm in 0.5-mm interval) at 2 mm caudal to bregma and 1.5 mm to midline. Reference screws were placed on frontal cortex. Local field potential (LFP) was collected by OmniPlex Neural Recording Data Acquisition System (Plexon, RRID: SCR_014803) with 2000 sampling rate filtered by low pass at 100 Hz. Data were analyzed by MATLAB in customized code.

BrdU injection and quantification of neural stem/progenitor cells (NSPCs)

For proliferation assay, mice were received a single-pulse of BrdU (50 mg/kg; Sigma-Aldrich) injection. After 2 h, mice were perfused with 4% paraformaldehyde in PBS (pH 7.4), and brain tissues were collected. For quantification of neuronal differentiation, mice were injected six times intraperitoneally with BrdU at 12-h intervals and killed by transcardial perfusion two weeks after their final BrdU injection. For quantification of the survival of newly generated DGCs, mice were injected six times intraperitoneally with BrdU at 12-h intervals before tDCS application and killed by transcardial perfusion 40 d after their final BrdU injection. For quiescent NSPC pool quantification, mice were killed 2 h after a single-pulse of 5-ethynyl-2-deoxyuridine (EdU; 50 mg/kg; Abcam) injection. Experimental designs are summarized in Figure 1*A*. The dorsal DG (bregma from −1.0 to −2.3 mm) and

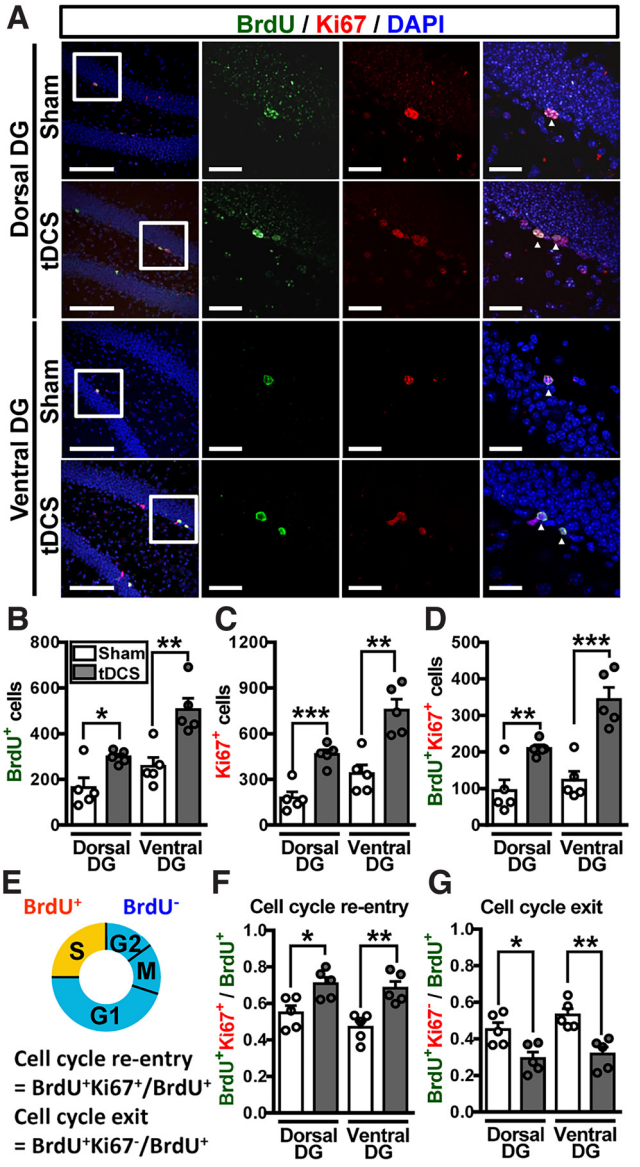

Figure 2. Multisession anodal tDCS treatment increases NSPC proliferation by enhancing cell cycle reentry and decreasing cell cycle exit. ***A***, Representative immunofluorescence images of dorsal and ventral hippocampal DG sections from sham-treated and tDCS-treated mice triple stained for BrdU (green), Ki67 (red), and DAPI (blue) 2 h after BrdU injection. Middle and right panels are higher-magnification views of the boxed areas in the left panel. The white arrowhead indicates $BrdU^+Ki67^+DAPI^+$ cells. Scale bar: 100 μm for the left panel, 25 μm for the middle and right panels. ***B***, Quantification of the total number of $BrdU^+$ cells in dorsal and ventral DG of sham-treated and tDCS-treated mice 2 h after BrdU injection (two-tailed unpaired Student's *t* test, Dorsal DG, $t_{(8)} = 3.00$, $p = 0.016$; Ventral DG, $t_{(8)} = 3.93$, $p = 0.004$; $n = 5$ in each group). ***C***, Quantification of the total number of $Ki67^+$ cells in dorsal and ventral DG of sham-treated and tDCS-treated mice 2 h after BrdU injection (two-tailed unpaired Student's *t* test, Dorsal DG, $t_{(8)} = 5.69$, $p < 0.001$; Ventral DG, $t_{(8)} = 4.57$, $p = 0.001$; $n = 5$ in each group). ***D***, Quantification of the total number of $BrdU^+Ki67^+$ cells in dorsal and ventral DG of sham-treated and tDCS-treated mice 2 h after BrdU injection (two-tailed unpaired Student's *t* test, Dorsal DG, $t_{(8)} = 3.73$, $p = 0.005$; Ventral DG, $t_{(8)} = 5.35$, $p < 0.001$; $n = 5$ in each group). ***E***, Schematic representation of the analysis of cell-cycle kinetics by a BrdU/Ki67 double labeling and of the indexes used for cell cycle reentry and exit. ***F***, Increased proportion of cell cycle reentry in dorsal and ventral DG of tDCS-treated mice (two-tailed unpaired Student's *t* test, Dorsal DG, $t_{(8)} = 3.04$, $p = 0.016$; Ventral DG, $t_{(8)} = 4.20$, $p = 0.003$; $n = 5$ in each group). ***G***, Reduced proportion of cell cycle exit in dorsal and ventral DG of tDCS-treated mice (two-tailed unpaired Student's *t* test, Dorsal DG, $t_{(8)} = 3.04$, $p = 0.016$; Ventral DG, $t_{(8)} = 4.20$, $p = 0.003$; $n = 5$ in each group). Data are presented as mean ± SEM, $^*p < 0.05$, $^{**}p < 0.01$, and $^{***}p < 0.001$ as compared with sham group.

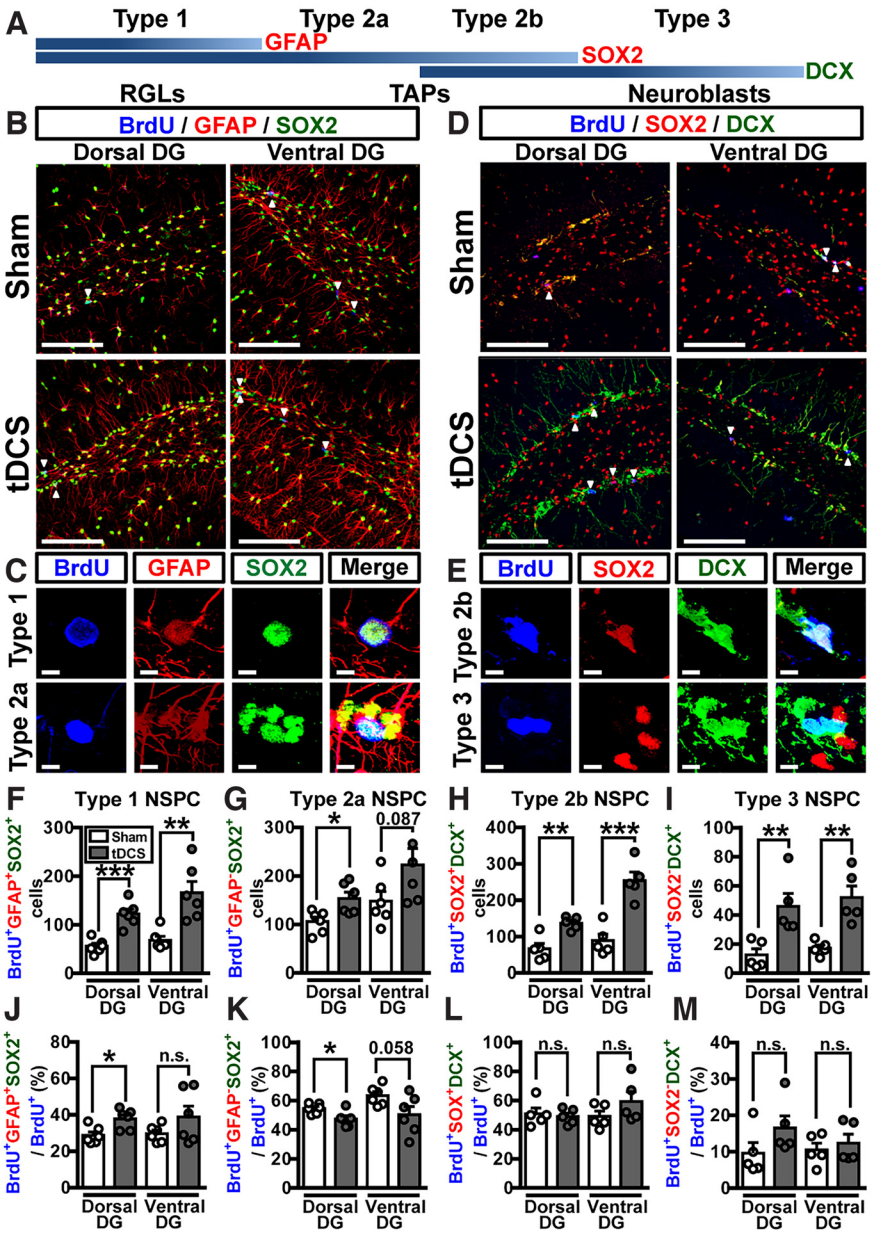

Figure 3. Effects of multisession anodal tDCS treatment on individual NSPC populations. ***A***, Schematic depiction of lineage-specific markers for distinguishing individual NSPC populations. The NSPC niche is comprised of type 1 ($BrdU^+GFAP^+SOX2^+$) radial glia-like stem cells (RGLs), type 2a ($BrdU^+GFAP^-SOX2^+$) and type 2b ($BrdU^+SOX2^+DCX^+$) transient amplifying progenitor cells (TAPs) and type 3 ($BrdU^+SOX2^-DCX^+$) neuroblasts. ***B***, Representative immunofluorescence images of dorsal and ventral hippocampal DG sections from sham-treated and tDCS-treated mice triple stained for BrdU (blue), GFAP (red), and SOX2 (green) 2 h after BrdU injection. The white arrowhead indicates $BrdU^+GFAP^+SOX^+$ cells. Scale bar: 100 μm. ***C***, Representative immunofluorescence images of type 1 and type 2a NSPCs. Scale bar: 5 μm. ***D***, Representative immunofluorescence images of dorsal and ventral hippocampal DG sections from sham-treated and tDCS-treated mice triple stained for BrdU (blue), SOX2 (red), and DCX (green) 2 h after BrdU injection. The white arrowhead indicates $BrdU^+SOX^+DCX^+$ cells. Scale bar: 100 μm. ***E***, Representative immunofluorescence images of type 2b and type 3 NSPCs. Scale bar: 5 μm. ***F***, Quantification of the total number of type 1 NSPC in dorsal and ventral DG of sham-treated and tDCS-treated mice (two-tailed unpaired Student's *t* test, Dorsal DG, $t_{(10)} = 5.57$, $p < 0.001$; Ventral DG, $t_{(10)} = 3.97$, $p = 0.002$; $n = 6$ in each group). ***G***, Quantification of the total number of type 2a NSPC in dorsal and ventral DG of sham-treated and tDCS-treated mice (two-tailed unpaired Student's *t* test, Dorsal DG, $t_{(10)} = 2.97$, $p = 0.014$; Ventral DG, $t_{(10)} = 1.90$, $p = 0.087$; $n = 6$ in each group). ***H***, Quantification of the total number of type 2b NSPC in dorsal and ventral DG of sham-treated and tDCS-treated mice (two-tailed unpaired Student's *t* test, Dorsal DG, $t_{(8)} = 4.19$, $p = 0.003$; Ventral DG, $t_{(8)} = 5.61$, $p < 0.001$; $n = 5$ in each group). ***I***, Quantification of the total number of type 3 NSPC in dorsal and ventral DG of sham-treated and tDCS-treated mice (two-tailed unpaired Student's *t* test, Dorsal DG, $t_{(8)} = 3.38$, $p = 0.009$; Ventral DG, $t_{(8)} = 4.19$, $p = 0.003$; $n = 5$ in each group). ***J***, Quantification of the percentage of type 1 NSPC out of the total $BrdU^+$ cells in dorsal and ventral DG of sham-treated and tDCS-treated mice (two-tailed unpaired Student's *t* test, Dorsal DG, $t_{(10)} = 3.10$, $p = 0.011$; Ventral DG, $t_{(10)} = 1.47$, $p = 0.172$; $n = 6$ in each group). ***K***, Quantification of the percentage of type 2a NSPC out of the total $BrdU^+$ cells in dorsal and ventral DG of sham-treated and tDCS-treated mice (two-tailed unpaired Student's *t* test, Dorsal DG, $t_{(10)} = 2.80$, $p = 0.018$; Ventral DG, $t_{(10)} = 2.14$, $p = 0.058$; $n = 6$ in each group). ***L***, Quantification of the percentage of type 2b NSPC out of the total $BrdU^+$ cells in dorsal and ventral DG of sham-treated and tDCS-treated mice (two-tailed unpaired Student's *t* test, Dorsal DG, $t_{(8)} = 0.39$, $p = 0.705$; Ventral DG, $t_{(8)} = 1.35$, $p = 0.214$; $n = 5$ in each group). ***M***, Quantification of the percentage of type 3 NSPC out of the total $BrdU^+$ cells in dorsal and ventral DG of sham-treated and tDCS-treated mice (two-tailed unpaired Student's *t* test, Dorsal DG, $t_{(8)} = 1.58$, $p = 0.153$; Ventral DG, $t_{(8)} = 0.61$, $p = 0.557$; $n = 5$ in each group). Data are presented as mean ± SEM, $^*p < 0.05$, $^{**}p < 0.01$, and $^{***}p < 0.001$ as compared with sham group. n.s.: not significant.

ventral DG (bregma from −2.4 to −4.0 mm) of the hippocampus were sectioned coronally at a thickness of 40 μm using a sliding microtome (SM2010R; Leica Microsystems).

Fluorescent immunolabelling was used for counting numbers of NSPCs. For $BrdU^+/Ki67^+$, $BrdU^+$/doublecortin $(DCX)^+$, $BrdU^+$/neuronal nuclear protein $(NeuN)^+$, $BrdU^+$/Glial fibrillary acidic protein $(GFAP)^+$SRY-box transcription factor 2 $(SOX2)^+$ and $BrdU^+SOX2^+DCX^+$ labeling, free-floating sections were denatured in 10 mM saline-sodium citrate buffer at 85°C for 30 min and then incubated at 37°C for 30 min in 1 N HCl. Sections were rinsed twice for 10 min at 25°C in 0.1 M Na borate (pH 8.5) and then incubated in the primary antibodies against BrdU (1:500; Millipore, catalog #MAB4072, RRID:AB_95024), Ki67 (1:1000; Abcam, catalog #ab15580), DCX (1:1000; Millipore, catalog #AB2253, RRID:AB_1586992), NeuN (1:2000; Millipore, ABN78, RRID:AB_10807945), GFAP (1:1000; Invitrogen, catalog #13–0300, RRID:AB_2532994), or SOX2 (1:1000; Abcam, catalog #ab97959, RRID:AB_2341193) overnight at 4°C in PBS with 0.3% Triton X-100 and 30% bovine serum albumin (BSA). Finally, sections were washed in PBS with 0.4% Triton and then incubated with the Alexa Fluor 405-conjugated, 488-conjugated, or 568-conjugated secondary antibodies [Thermo Fisher Scientific, catalog #A48255 (RRID:AB_2890536), A-11 073 (RRID:AB_2534117)/A-11 034 (RRID:AB_2576217)/A-11 001 (RRID:AB_2534069), A-11 075 (RRID:AB_141954)/A-11 036 (RRID:AB_10563566)/A-11 004 (RRID:AB_2534072)/A-11 077 (RRID:AB_2534121)] for 2 h at room temperature. For EdU labeling, slices were incubated in EdU click reaction buffer [0.4% Triton X-100, 1 mM CuSO4, 100 μM 488 Alexa azide fluorescent-azide (Thermo Fisher Scientific, catalog #A10266, RRID:AB_2757794), and 100 mM ascorbic acid] for 30 min as described previously with minor modification (Salic and Mitchison, 2008). The nuclei were visualized using mounting medium with 4',6-diamidino-2-phenylindole (DAPI; Abcam, catalog #ab104139). The immunostained sections were collected on separate gelatin-subbed glass slides, rinsed extensively in PBS and mounted with Fluoromount-G Mounting Medium (Invitrogen, catalog #00-4958-02, RRID:SCR_015961).

Quantification of BrdU-labeled cells was performed using a modified unbiased stereology

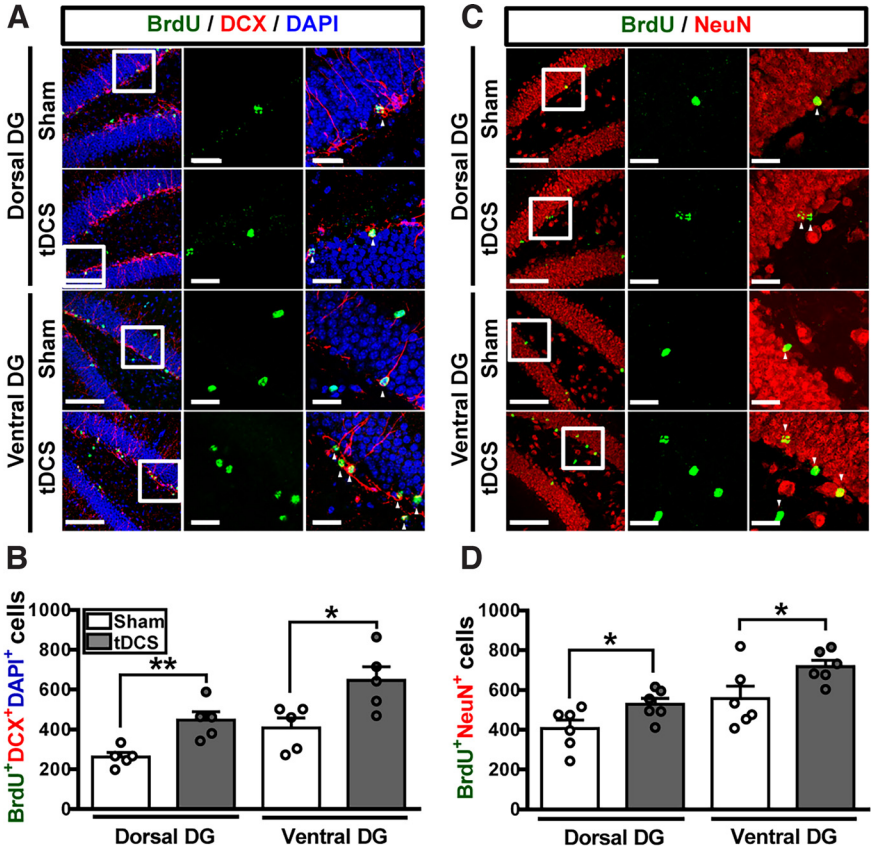

Figure 4. Multisession anodal tDCS treatment enhances the differentiation and survival of NSPCs. ***A***, Representative immunofluorescence images of dorsal and ventral hippocampal DG sections from sham-treated and tDCS-treated mice triple stained for BrdU (green), DCX (red), and DAPI (blue) 14 d after last BrdU injection. Middle and right panels are higher-magnification views of the boxed areas in the left panel. The white arrowhead indicates $BrdU^+DCX^+DAPI^+$ cells. Scale bar: 100 μm for the left panel, 5 μm for the middle and right panels. ***B***, Quantification of the total number of $BrdU^+DCX^+DAPI^+$ cells in dorsal and ventral DG of sham-treated and tDCS-treated mice at 14 d after last BrdU injection (two-tailed unpaired Student's *t* test, Dorsal DG, $t_{(8)} = 3.88$, $p = 0.004$; Ventral DG, $t_{(8)} = 2.81$, $p = 0.022$; $n = 5$ in each group). ***C***, Representative immunofluorescence images of dorsal and ventral hippocampal DG sections from sham-treated and tDCS-treated mice double stained for BrdU (green) and NeuN (red) 28 d after last BrdU injection. Middle and right panels are higher-magnification views of the boxed areas in the left panel. The white arrowhead indicates $BrdU^+NeuN^+$ cells. Scale bar: 100 μm for the left panel, 5 μm for the middle and right panels. ***D***, Quantification of the total number of $BrdU^+NeuN^+$ cells in dorsal and ventral DG of sham-treated and tDCS-treated mice at 40 d after last BrdU injection (two-tailed unpaired Student's *t* test, Dorsal DG, $t_{(10)} = 2.312$, $p = 0.043$; Ventral DG, $t_{(10)} = 2.26$, $p = 0.047$; $n = 6$ in each group). Data are presented as mean ± SEM $^*p < 0.05$ and $^{**}p < 0.01$ as compared with sham group.

protocol as described previously (Lin et al., 2017). The fluorescence intensity of $BrdU^+$ cells was set at least twofold above the background. Every sixth section covering the entire DG of the hippocampus was processed for BrdU immunohistochemistry. All BrdU-labeled cells in the granule cell layer, subgranular zone (SGZ) and hilus were counted under fluorescent illumination at 400× using an Olympus BX51 microscope coupled to an Olympus DP70 digital camera. Total cell numbers were estimated by multiplying the number of cells counted in every sixth section by six. Fluorescence microscopic images were obtained using an Olympus FluoView FV3000 confocal microscope (Olympus Corporation).

The balance between cell cycle reentry and exit was determined using BrdU/Ki67 immunolabeling as described previously (Chenn and Walsh, 2002). To quantify cell proliferation, the number of proliferating radial neural stem cells (rNSC, $BrdU^+Ki67^+$ cells) was counted. To assess the extent of NSPC populations, the numbers of $BrdU^+GFAP^+SOX2^+$ (type 1), $BrdU^+GFAP^-SOX2^+$ (type 2a), $BrdU^+SOX2^+DCX^+$ (type 2b), and $BrdU^+SOX2^-DCX^+$ (type 3) cells were counted. The proliferating neuroblasts were identified based on the expression of both BrdU and DCX. Cell survival was determined by measuring the number of $BrdU^+NeuN^+$ cells. The quiescent NSPC pool was assessed by measuring the number of $EdU^-Nestin^+$ cells. All images were imported into NIH ImageJ software (RRID:SCR_001935) for analysis, and all the parameters used were kept consistent during capturing.

Hippocampal slice preparations and electrophysiology

Slice preparations and whole-cell patch-clamp recordings were performed as described previously (Lin et al., 2017). Briefly, mice were deeply anesthetized with 5% isoflurane and killed by decapitation. The brain was removed and quickly placed in ice-cold oxygenated choline-based cutting solution containing the following (in mM): 110 choline chloride, 2.5 KCl, 0.5 $CaCl_2$, 7 $MgSO_4$, 1.3 NaH_2PO_4, 25 $NaHCO_3$, 20 glucose, 5.5 kynurenic acid, 1.3 sodium ascorbate, 3 sodium pyruvate and saturated with 95% O_2 and 5% CO_2. Coronal slices containing dorsal or ventral hippocampus (250 μm) were prepared using a vibrating microtome (VT1200S; Leica Biosystems, Wetzlar, Germany) and immediately transferred to a holding chamber of artificial CSF (aCSF) containing (in mM): 117 NaCl, 4.7 KCl, 2.5 $CaCl_2$, 1.2 $MgCl_2$, 25 $NaHCO_3$, 1.2 NaH_2PO_4, and 11 glucose, pH 7.3–7.4, and saturated with 95% O_2 and 5% CO_2 and then kept at room temperature (~25°C) for at least 1 h before starting recordings. One slice was transferred to a submersion-type recording chamber and continuously perfused with oxygenated aCSF at a flow rate of 2–3 ml/min at ~32°C on a fixed-stage. Whole-cell patch-clamp recordings were made from visualized dentate granule cells (DGCs) using an Axopatch 200B amplifier (Molecular Devices, RRID:SCR_018866). Data acquisition and analysis were performed using a digitizer (Digidata 1440A, Molecular Devices, RRID:SCR_021038) and pCLAMP 9 software (Molecular Devices). The composition of intracellular solution was (in mM): 135 CsCl, 10 HEPES, 0.1 EGTA, 4 $MgCl_2$, 4 MgATP, 0.3 Na_3GTP, 7 phosphocreatine (pH 7.2). Tonic and phasic GABAergic inhibition were recorded with cells being held at −65 mV with existence of tetrodotoxin (TTX; 0.5 μM; Sigma-Aldrich), 6-cyano-7-nitroquinoxaline-2,3-dione (CNQX; 20 μM; Tocris Bioscience), and 2-amino-5-phosphonovaleric acid (APV; 50 μM; Tocris Bioscience) in the external solution. Bath application of the $GABA_A$ receptor blocker SR-95531 (100 μM; Tocris Bioscience) revealed tonic activity of $GABA_A$ receptors. Tonic GABAergic current was calculated as the baseline current after adding SR-95531. To ensure that miniature IPSCs (mIPSCs) were not included in the measurement of tonic inhibition, the mean value from the Gaussian fit was used as the value for the baseline tonic currents as described previously (Engin et al., 2015). Miniature EPSCs (mEPSCs) were recorded at a holding potential of −70 mV in the presence of TTX (0.5 μM) and SR-95531 (20 μM) and the composition of intracellular solution was (in mM): 135 K-gluconate, 5 KCl, 20 HEPES, 0.5 $CaCl_2$, 5 EGTA, and 5 MgATP (pH 7.2). The frequency and amplitude of mEPSCs and mIPSCs were analyzed off-line using a commercially available software (Mini Analysis 4.3; Synaptosoft) as previously described (Lin et al., 2017). Means were calculated from 3-min epochs recorded. Detection threshold for analysis was set at two times the root mean square of the background noise, and each event was further confirmed by visual inspection after detection.

Contextual fear discrimination task

The contextual fear discrimination task was performed using a computer-controlled context conditioning system (ENV-307A, MED Associates) as described previously (Jones et al., 2016) with minor modification. Mice were trained to discriminate between two similar contexts, A and B, through repeated experience in each context. Context A (the conditioning context) was a chamber (15.9 × 14.0 × 12.7 cm) consisting of a stainless-steel grid floor, aluminum side walls, a clear Plexiglas front door and white back wall. Context A was indirectly illuminated with a 12-W light bulb. The features of Context B (the safe context) were the same as those of Context A, except for black spots on the walls and a stainless-steel mesh floor. Each context was thoroughly cleaned with 70% ethanol after each trial to prevent bias based on olfactory cues. On the first 3 d (contextual fear acquisition), mice were placed in the Context A for 3 min to explore the environment and then received a single footshock (0.65 mA for 2 s). Mice were returned to their homecage 1 min after the footshock. Mice were subsequently trained to discriminate between these two contexts by being placed in the two contexts daily with 6-h interval in a pseudorandomized order for 10 d (from day 4 to day 13, discrimination task). Mice always received a footshock 3 min after being placed in Context A but not B. Freezing was scored as the total time spent freezing in each context during the first 3 min after being placed in Contexts A and B. Significant motion pixel (SMP) values are a linear measure of motion between frames captured at 7.5 Hz. Freezing level was defined as SMP < 20 for at least 1 s with the Freezeview software (MED Associates). The discrimination ratio was calculated as (freezing in Context A – freezing in Context B)/(freezing in Context A + freezing in Context B).

Drug administration

Rac-BHFF (Tocris Bioscience), a selective positive allosteric modulator of $GABA_B$ receptors, was dissolved in a mixture containing 15% dimethylsulfoxide (DMSO), 30% polyethylene glycol (PEG) and 50% saline (0.9% NaCl). Vehicle was a mixture containing 15% DMSO, 30% PEG, and 50% saline. Mice received intraperitoneal injection of vehicle or Rac-BHFF (30 mg/kg) 30 min before BrdU administration. The dose of Rac-BHFF was chosen on the basis of previous study (Malherbe et al., 2008). The DNA alkylating agent temozolomide (TMZ; Sigma-Aldrich) was administered intraperitoneally before the application of sham or tDCS at 25 mg/kg (PBS with 10% DMSO) per day for the first three consecutive days during sham or tDCS application according to previous protocol (Garthe et al., 2009; Stone et al., 2011). A total of two rounds of treatment (4 d apart) were administered to mice. Vehicle solution was the identical DMSO/PBS solution but without TMZ.

Brain-derived neurotrophic factor (BDNF) immunoassay

Mice were deeply anesthetized with 5% isoflurane and decapitated 1 or 28 d after last stimulation. Dorsal (bregma from −1.0 to −2.3 mm) and ventral (bregma from −2.4 to −4.0 mm) DG tissues were extracted and lysed in protein extraction reagent (Thermo Fisher Scientific, catalog #78501) containing proteinase and phosphatase single-use inhibitor cocktail (Thermo Fisher Scientific, catalog #78442). Total protein concentration was determined with Pierce BCA protein assay kit (Thermo Fisher Scientific, catalog #23225). The

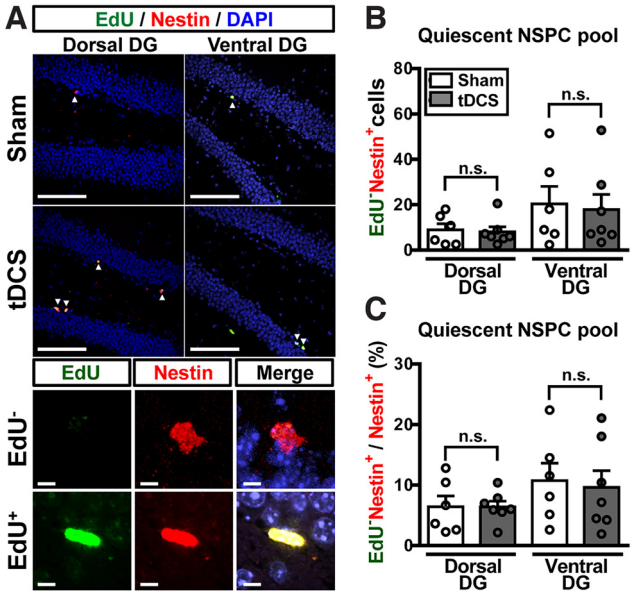

Figure 5. Effect of multisession anodal tDCS treatment on quiescent NSPC pool. ***A***, Representative immunofluorescence images of dorsal and ventral hippocampal DG sections from sham-treated and tDCS-treated mice triple stained for EdU (green), Nestin (red), and DAPI (blue) 2 h after EdU injection. The white arrowhead indicates $Nestin^+DAPI^+$ cells. Scale bar: 100 μm for the upper panels, 5 μm for the lower panels. ***B***, Quantification of the total number of quiescent NSPCs ($EdU^-Nestin^+$) in dorsal and ventral DG of sham-treated and tDCS-treated mice 2 h after EdU injection (two-tailed unpaired Student's *t* test, Dorsal DG, $t_{(11)} = 0.24$, $p = 0.813$; Ventral DG, $t_{(11)} = 0.25$, $p = 0.81$; Sham, $n = 6$; tDCS, $n = 7$). ***C***, Quantification of the percentage of quiescent NSPCs ($EdU^-Nestin^+$) out of the total $Nestin^+$ cells in dorsal and ventral DG of sham-treated and tDCS-treated mice (two-tailed unpaired Student's *t* test, Dorsal DG, $t_{(11)} = 0.004$, $p = 0.996$; Ventral DG, $t_{(11)} = 0.27$, $p = 0.788$; Sham, $n = 6$; tDCS, $n = 7$). Data are presented as mean ± SEM n.s.: not significant.

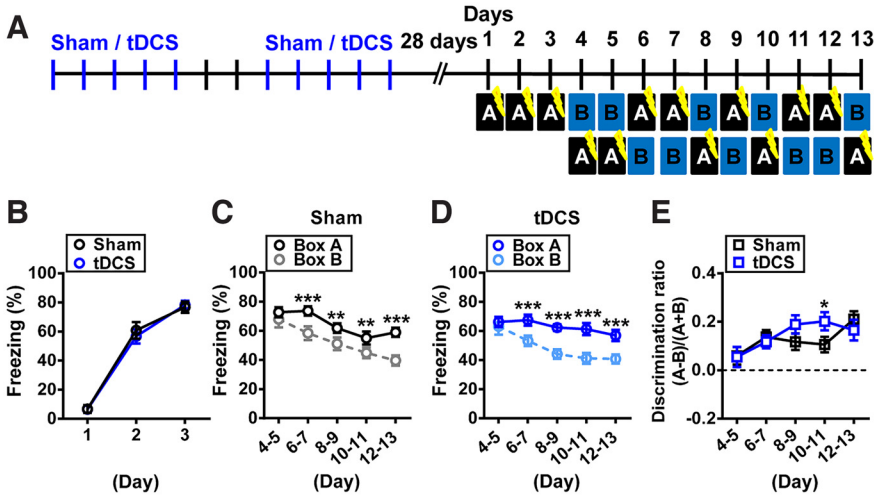

Figure 6. Multisession anodal tDCS treatment enhances contextual fear discrimination. ***A***, Experimental procedure for the contextual fear discrimination learning task. ***B***, Summary graph showing the percentage of freezing during first 3 d in Context A (conditioning context; two-way repeated measure ANOVA, Group: $F_{(1,16)} = 0.108$, $p = 0.746$; Time: $F_{(2,32)} = 307.3$, $p < 0.0001$; Interaction: $F_{(2,32)} = 1.061$, $p = 0.358$; $n = 17$ in each group). ***C***, Summary graph showing the percentage of freezing from day 4 to day 13 in Context A and Context B (unconditioning context) of sham-treated group (two-way repeated measure ANOVA, Group: $F_{(1,16)} = 51.04$, $p < 0.0001$; Time: $F_{(4,64)} = 31.71$, $p < 0.0001$; Interaction: $F_{(4,64)} = 3.765$, $p = 0.008$; $n = 17$ in each group; Bonferroni's *post hoc* multiple comparisons test, days 6–7: $p < 0.0001$, days 8–9: $p = 0.0016$, days 10–11: $p = 0.0033$, days 12–13: $p < 0.0001$); $^{**}p < 0.01$, $^{***}p < 0.001$ as compared with box ***B***. ***D***, Summary graph showing the percentage of freezing from day 4 to day 13 in Context A and Context B of tDCS-treated group (two-way repeated measure ANOVA, Group: $F_{(1,16)} = 49.58$, $p < 0.0001$; Time: $F_{(4,64)} = 8.849$, $p < 0.0001$; Interaction: $F_{(4,64)} = 5.356$, $p = 0.0009$; $n = 17$ in each group; Bonferroni's *post hoc* multiple comparisons test, days 6–7: $p < 0.0001$, days 8–9: $p < 0.0001$, days 10–11: $p < 0.0001$, days 12–13: $p < 0.0001$); $^{***}p < 0.001$ as compared with box ***B***. ***E***, Summary graph showing the contextual discrimination ratio from day 4 to day 13 in sham-treated and tDCS-treated group (two-way repeated measure ANOVA, Group: $F_{(1,16)} = 0.416$, $p = 0.528$; Time: $F_{(4,64)} = 4.992$, $p = 0.0014$; Interaction: $F_{(4,64)} = 2.822$, $p = 0.032$; $n = 17$ in each group; Bonferroni's *post hoc* multiple comparisons test, days 10–11: $p = 0.0499$). Data are presented as mean ± SEM, $^{*}p < 0.05$ as compared with sham group.

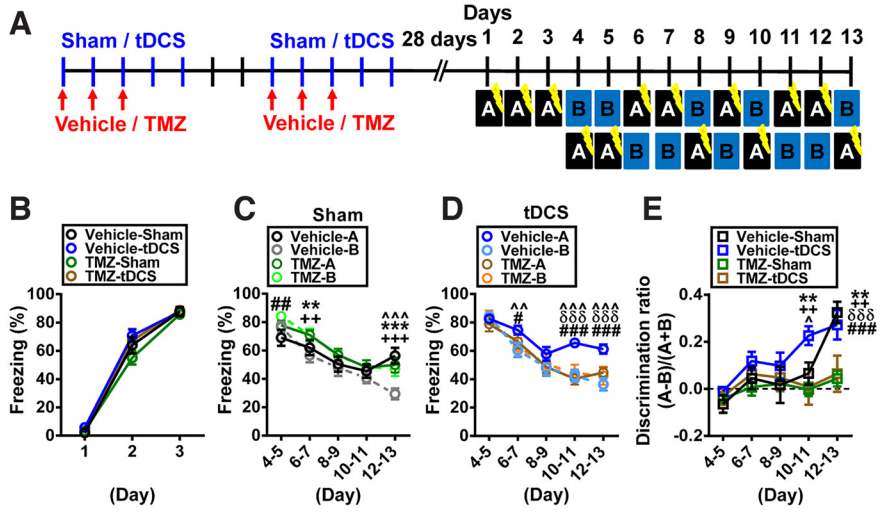

Figure 7. Suppression of AHN blocks tDCS-mediated enhancement of contextual fear discrimination enhancement. ***A***, Experimental procedure for the contextual fear discrimination task and TMZ application. ***B***, Summary graph showing the percentage of freezing during first 3 d in Context A (two-way repeated measure ANOVA, Group: $F_{(3,30)} = 1.394$, $p = 0.2638$; Time: $F_{(2,20)} = 484.8$, $p < 0.0001$; Interaction: $F_{(6,60)} = 0.8650$, $p = 0.5259$; $n = 11$ in each group). ***C***, Summary graph showing the percentage of freezing from day 4 to day 13 in Context A and Context B of Vehicle-treated and TMZ-treated sham groups (two-way repeated measure ANOVA, Group: $F_{(3,30)} = 1.609$, $p = 0.2079$; Time: $F_{(4,40)} = 75.12$, $p < 0.0001$; Interaction: $F_{(12,120)} = 3.389$, $p = 0.0003$; $n = 11$ in each group; Bonferroni's *post hoc* multiple comparisons test, days 4–5: $\#\#p_{\text{Vehicle context B versus TMZ context A}} = 0.0033$; days 6–7: $^{**}p_{\text{Vehicle context B versus TMZ context A}} = 0.0057$, $++p_{\text{Vehicle context B versus TMZ context B}} = 0.0057$; days 12–13: $\wedge\wedge\wedge p_{\text{Vehicle context A versus Vehicle context B}} < 0.0001$, $^{***}p_{\text{Vehicle context B versus TMZ context A}} < 0.0001$, $+++p_{\text{Vehicle context B versus TMZ context B}} = 0.0004$). ***D***, Summary graph showing the percentage of freezing from day 4 to day 13 in Context A and Context B of Vehicle-treated and TMZ-treated tDCS groups (two-way repeated measure ANOVA, Group: $F_{(3,30)} = 3.696$, $p = 0.0224$; Time: $F_{(4,40)} = 54.89$, $p < 0.0001$; Interaction: $F_{(12,120)} = 3.502$, $p = 0.0003$; $n = 11$ in each group; Bonferroni's *post hoc* multiple comparisons test, days 6–7: $\wedge\wedge p_{\text{Vehicle context A versus Vehicle context B}} = 0.0030$, $\#p_{\text{Vehicle context A versus TMZ context B}} = 0.0183$; days 10–11: $\wedge\wedge\wedge p_{\text{Vehicle context A versus Vehicle context B}} < 0.0001$, $\delta\delta\delta p_{\text{Vehicle context A versus TMZ context A}} < 0.0001$, $\#\#\#p_{\text{Vehicle context A versus TMZ context B}} < 0.0001$; days 12–13: $\wedge\wedge\wedge p_{\text{Vehicle context A versus Vehicle context B}} < 0.0001$, $\delta\delta\delta p_{\text{Vehicle context A versus TMZ context A}} = 0.0003$, $\#\#\#p_{\text{Vehicle context A versus TMZ context B}} < 0.0001$). ***E***, Summary graph showing the contextual discrimination ratio from day 4 to day 13 in Vehicle-treated or TMZ-treated sham and tDCS groups (two-way repeated measure ANOVA, Group: $F_{(3,30)} = 4.537$, $p = 0.0097$; Time: $F_{(4,40)} = 13.08$, $p < 0.0001$; Interaction: $F_{(12,120)} = 2.545$, $p = 0.005$; $n = 11$ in each group; Bonferroni's *post hoc* multiple comparisons test, days 10–11: $\wedge p_{\text{Vehicle-sham versus Vehicle-tDCS}} = 0.046$, $^{**}p_{\text{Vehicle-tDCS versus TMZ-sham}} = 0.0011$, $++p_{\text{Vehicle-tDCS versus TMZ-tDCS}} = 0.0021$; days 12–13: $\#\#\#p_{\text{Vehicle-sham versus TMZ-sham}} < 0.0001$, $\delta\delta\delta p_{\text{Vehicle-sham versus TMZ-tDCS}} = 0.0001$, $^{**}p_{\text{Vehicle-tDCS versus TMZ-sham}} = 0.0012$, $++p_{\text{Vehicle-tDCS versus TMZ-tDCS}} = 0.0040$). Data are presented as mean ± SEM.

BDNF precursor (proBDNF) and mature BDNF protein levels were determined with Mature BDNF/proBDNF Combo Rapid ELISA kit (Biosensis, catalog #BEK-2240) according to the manufacturer's protocol as previously described (Wu et al., 2017; Yu et al., 2019).

Statistical analysis

Sample sizes were based on previous work of a similar nature by our laboratory (Wu et al., 2017; Yu et al., 2019) and determined with power analysis (a two-tailed analysis with a significance set at $\alpha = 0.05$ and power $\geq 80\%$; G*Power software). No specific randomization method was used. Animals were randomly allocated into different experimental groups. All results are presented as means ± SEM and analyzed by the GraphPad Prism 6 software (GraphPad Software Inc.). Normality of data distribution was verified using the Shapiro–Wilk test normality test. Two-tailed unpaired Student's *t* test or two-tailed Mann–Whitney *U* test was used to compare differences between two independent groups. The difference between multiple groups was calculated by two-way ANOVA followed by Bonferroni's *post hoc* analyses. Number of animals used is indicated by *n*. Differences were considered as significant at $p < 0.05$. The sample sizes and statistical analysis details for each figure are reported in the corresponding figure legend.

Results

Multisession anodal tDCS increases NSPC proliferation

It is known that the effects of a single session of tDCS is often quite variable and short-lived, whereas multiple, spaced sessions may increase the duration of effects (Reis et al., 2009). The present study was undertaken to investigate the long-term impact of multisession anodal tDCS on AHN. Experimental designs are summarized in Figure 1*A*. We also determined the actual electric field gradient along the hippocampal brain tissue imposed by tDCS application in our experimental design. Mice were prepared for LFP recording in the dorsal hippocampus in alert condition during simultaneous application of tACS at 1 Hz (Fig. 1*B*). Sequential recordings were obtained every 0.5 mm from alveus hippocampus −1 to −2.5 mm depth. Figure 1*C* shows the sampling responses to tACS stimulation obtained from recordings at different depths. The calculated electric fields at different depths and intensities are shown in Figure 1*D*. The magnitude of the electric field decreased with depth for the tested intensities.

AHN is highly dynamic and can be divided into multiple stages including cell proliferation, neuronal differentiation and maturation (Christian et al., 2014). To determine whether multisession anodal tDCS may influence proliferation of NSPCs, sham-treated and tDCS-treated mice were subjected to a single intraperitoneal injection of BrdU, and double fluorescent labeling for detection of BrdU-positive ($BrdU^+$) proliferating cells ($Ki67^+$) was performed on both dorsal and ventral hippocampal DG sections 2 h later (Fig. 2*A*). Stereological analysis revealed statistically significant increases in the total number of $BrdU^+$ (Fig. 2*B*), $Ki67^+$ (Fig. 2*C*), and $BrdU^+Ki67^+$ (Fig. 2*D*) cells in both dorsal and ventral DG of tDCS group compared with sham group. To determine whether multisession anodal tDCS affects cell cycle progression in NSPCs, the number of cells re-entering ($BrdU^+Ki67^+/BrdU^+$) and exiting the cell cycle ($BrdU^+Ki67^-/BrdU^+$) was calculated (Fig. 2*E*). As shown in Figure 2*F*, the proportion of cell cycle reentry was significantly increased in tDCS group compared with sham group. In contrast, a significant lower proportion of cells were observed to exit cell cycle in tDCS group compared with sham group (Fig. 2*G*).

Since adult hippocampal NSPCs are composed of three major cell subtypes, radial glia-like precursor cells (type 1), transiently amplifying progenitor cells (type 2a and 2b) and neuroblasts (type 3; Kempermann et al., 2015), we next assessed which NSPC population(s) was affected. To do this, we analyzed the number of cells that are positive for GFAP and SOX2, markers of neural stem and progenitor cells, respectively (Suhet al., 2007; Lugert et al., 2010; Fig. 3*A*). Consistently, we found significant increases in the total number of type 1 radial glia-like cells ($BrdU^+GFAP^+SOX2^+$; Fig. 3*B*,*C*,*F*) and type 2a amplifying progenitor cells ($BrdU^+GFAP^-SOX2^+$; Fig. 3*G*) in dorsal DG, as well as type 2b amplifying progenitor cells ($BrdU^+SOX2^+DCX^+$; Fig. 3*D*,*E*,*H*) and type 3 neuroblasts ($BrdU^+SOX2^-DCX^+$; Fig. 3*I*) in both dorsal and ventral DG of tDCS group compared with sham

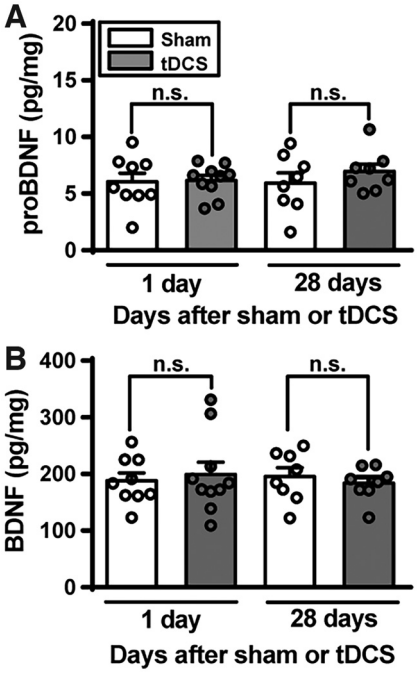

Figure 8. The expression levels of proBDNF and mature BDNF are not altered by multisession anodal tDCS treatment. ***A***, Quantification of the protein level of proBDNF 1 and 28 d after sham or tDCS treatments in the DG of the hippocampus (two-tailed unpaired Student's *t* test, 1 d: $t_{(17)} = 0.14$, $p = 0.889$; Sham, $n = 9$; tDCS, $n = 10$; 28 d: $t_{(14)} = 0.93$, $p = 0.37$; $n = 8$ in each group). ***B***, Quantification of the protein level of BDNF 1 and 28 d after sham or tDCS treatments in the DG of the hippocampus (two-tailed unpaired Student's *t* test, 1 d: $t_{(17)} = 0.41$, $p = 0.689$; Sham, $n = 9$; tDCS, $n = 10$; 28 d: $t_{(14)} = 0.62$, $p = 0.546$, $n = 8$ in each group). Data are presented as mean ± SEM, n.s.: not significant.

group. Furthermore, we found a significant increase in the percentage of type 1 radial glia-like cells to total $BrdU^+$ cells in tDCS group compared with sham group (Fig. 3*J*). In contrast, the percentage of type 2a amplifying progenitor cells to total $BrdU^+$ cells was significantly decreased in tDCS group compared with sham group (Fig. 3*K*). Nevertheless, no significant differences were found between tDCS and sham groups in the percentages of type 2b amplifying progenitor cells (Fig. 3*L*) and type 3 neuroblasts (Fig. 3*M*) to total $BrdU^+$ cells in both dorsal and ventral DG.

Multisession anodal tDCS increases NSPC differentiation and survival

To assess whether multisession anodal tDCS may affect neuronal differentiation and survival of newly generated DGCs, sham and tDCS mice were subjected to multiple BrdU injections (Lin et al., 2017), and double fluorescent labeling for detection of BrdU and immature neurons (DCX^+) or mature neurons ($NeuN^+$) was performed on both dorsal and ventral hippocampal sections 14 or 40 d later. A significant increase in the total number of $BrdU^+DCX^+$ cells in tDCS group at 14 d after BrdU injection compared with sham group in both dorsal and ventral DG (Fig. 4*A*,*B*). To examine the effect of tDCS on the survival of newly generated DGCs, multiple BrdU injections were administered before tDCS application. Similarly, quantification of the total number of $BrdU^+NeuN^+$ cells revealed a significant increase in tDCS at 40 d after BrdU injection compared with sham group in both dorsal and ventral DG (Fig. 4*C*,*D*). These results indicate that multisession anodal tDCS can increase NSPC differentiation and newly generated DGC survival.

Multisession anodal tDCS does not affect quiescent NSPC Pool

To determine whether multisession anodal tDCS may accelerate the depletion of quiescent NSPC pool, sham and tDCS mice were subjected to multiple BrdU injections for 28 d to label newly generated DGCs in response to sham or tDCS treatment, followed by thymidine analog EdU injection on the last day to label the background proliferating cells, and double fluorescent labeling for detection of EdU-negative (EdU^-) quiescent NSPCs ($Nestin^+$), was performed on both dorsal and ventral hippocampal sections 2 h later. The total number of $EdU^-Nestin^+$ cells (Fig. 5*A*,*B*) and the percentage of $EdU^-Nestin^+$ cells to total $Nestin^+$ cells (Fig. 5*C*) were not significant different between tDCS and sham groups, suggesting that tDCS treatment does not alter quiescent NSPC pool.

Multisession anodal tDCS enhances contextual fear discrimination

AHN is functionally linked to modulate hippocampal memory interference, such as pattern separation (Clelland et al., 2009; Sahay et al., 2011). To further address the functional impact of tDCS-mediated enhancement of AHN, we then evaluated hippocampal memory interference using a contextual fear discrimination task. In this test, we subjected sham or tDCS mice to contextual fear conditioning using a pair of similar Context A and Context B. As shown in Figure 6*A*, on the first 3 d, mice were placed only into Context A, receiving a single footshock after 180 s. There was no difference between groups in the percentage of freezing during the learning phase (Fig. 6*B*). From day 4 to day 13, mice were placed in either Context A or B, where Context A is associated with a single footshock and Context B is not (Fig. 6*C*,*D*). Initially, both sham and tDCS groups cannot distinguish between contexts and thus exhibited similar freezing levels in both contexts (days 4–5). As the experiment progressed, both sham and tDCS mice gained to ability to discriminate Context B from Context A effectively, and the discrimination ratio increased (Fig. 6*C*–*E*). On days 10–11, tDCS group exhibited a significant enhancement in the acquisition of discrimination ability and showed a higher discrimination ratio than sham group (Fig. 6*E*), suggesting that tDCS treatment enhances context discrimination.

To further validate whether tDCS enhances context discrimination via a neurogenic mechanism, we examined the impact of inhibiting neurogenesis using the DNA-alkylating agent TMZ, which has been proven to suppress NSPC proliferation in the adult hippocampus (Garthe et al., 2009; Stone et al., 2011; Niibori et al., 2012). In this experiment, sham and tDCS mice were treated with vehicle or TMZ per day for the first three consecutive days during sham or tDCS application, with a total of two rounds. Four weeks after last trial of sham or tDCS application, mice were trained in the contextual fear discrimination task (Fig. 7*A*). There were no differences among groups in the percentage of freezing during the learning phase (Fig. 7*B*). During the course of subsequent tests, both vehicle-treated or TMZ-treated sham and tDCS groups cannot distinguish between contexts and thus exhibited similar freezing levels in both contexts on days 4–9 (Fig. 7*C*–*E*). As the experiment progressed, vehicle-treated tDCS group showed a significantly higher discrimination ratio than those of vehicle-treated sham, TMZ-treated sham and TMZ-treated tDCS groups on days 10–11 (Fig. 7*E*). In addition, we observed failed tDCS-enhancement of contextual fear discrimination in TMZ-treated mice. Only vehicle-treated sham

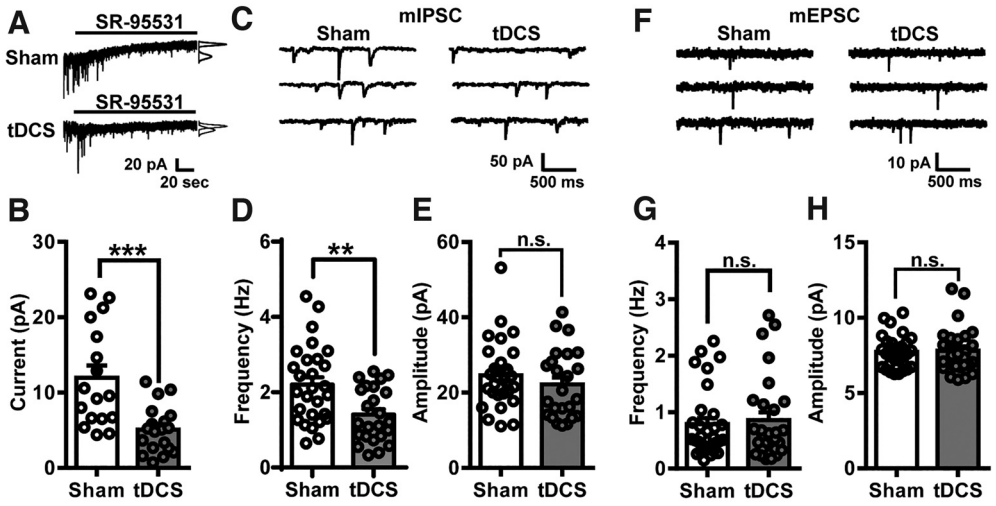

Figure 9. Multisession anodal tDCS treatment reduces GABAergic inhibitory tone in the DG of the hippocampus. Since there was no difference, electrophysiological data obtained from dorsal and ventral DG were combined. ***A***, Left, Representative traces recorded at a holding potential of −65 mV in DGCs from sham-treated and tDCS-treated group, followed by SR-95531 (100 μM) application. Right, All-points histogram and Gaussian fit from each segment. ***B***, Quantification of tonic GABA currents in DGCs from sham-treated and tDCS-treated mice (two-tailed unpaired Student's *t* test, $t_{(34)} = 4.08$, $p < 0.001$; Sham, $n = 17$ cells from 8 mice; tDCS, $n = 19$ cells from 8 mice). ***C***, Representative traces of mIPSCs in DGCs from sham-treated and tDCS-treated group. ***D***, Quantification of the frequency of mIPSCs in DGCs from sham-treated and tDCS-treated group (two-tailed unpaired Student's *t* test, $t_{(50)} = 3.21$, $p = 0.002$; Sham, $n = 28$ cells from 8 mice; tDCS, $n = 24$ cells from 8 mice). ***E***, Quantification of the amplitude of mIPSCs in DGCs from sham-treated and tDCS-treated group (two-tailed unpaired Student's *t* test, $t_{(50)} = 0.95$, $p = 0.35$; Sham, $n = 28$ cells from 8 mice; tDCS, $n = 24$ cells in 8 mice). ***F***, Representative traces of mEPSCs in DGCs from sham-treated and tDCS-treated group. ***G***, Quantification of the frequency of mEPSCs in DGCs from sham-treated and tDCS-treated group (two-tailed Mann–Whitney test, $U = 430$, $p = 0.95$; Sham, $n = 31$ cells from 5 mice; tDCS, $n = 28$ cells from 5 mice). ***H***, Quantification of the amplitude of mEPSCs in DGCs from sham-treated and tDCS-treated group (two-tailed unpaired Student's *t* test, $t_{(57)} = 0.19$, $p = 0.85$; Sham, $n = 31$ cells from 5 mice; tDCS, $n = 28$ cells from 5 mice). Data are presented as mean ± SEM, $^{**}p < 0.01$ and $^{***}p < 0.001$, n.s.: not significant.

and vehicle-treated tDCS groups can discriminate Context B from Context A on days 12–13 (Fig. 7*C–E*). These results indicate that AHN mediates the enhancing effect of tDCS on contextual fear discrimination.

Multisession anodal tDCS decreases GABAergic inhibitory tone in the DG

What is molecular mechanism subtending tDCS effect? Since anodal tDCS can exert its beneficial effects on memory modulation through upregulation of BDNF (Podda et al., 2016; Yu et al., 2019) and BDNF is known to subserve an important role in regulating AHN processes (Choi et al., 2018), we first assessed expression of proBDNF and BDNF in the DG following our multisession anodal tDCS paradigm. However, we observed no significant differences in proBDNF (Fig. 8*A*) and BDNF (Fig. 8*B*) protein levels between tDCS and sham groups 1 d or 28 d after treatment.

Given that the inhibitory neurotransmitter GABA has been identified as an important niche signal in regulating AHN (Song et al., 2012; Sibbe and Kulik, 2017), we next examined whether tDCS-mediated enhancement of AHN could be mediated by alterations of GABAergic neurotransmission in the DG. We found that the amplitudes of GABAergic tonic currents in DGCs were significantly reduced in tDCS group compared with sham group (Fig. 9*A*,*B*). Similarly, a significant decrease of fast synaptic GABAergic transmission was also observed in DGCs from tDCS group compared with sham group, manifested by a reduced mIPSC frequency (Fig. 9*C–E*). However, no significant difference was found between sham and tDCS groups in the frequency and amplitude of mEPSC (Fig. 9*F–H*), indicating a selective effect of tDCS on GABAergic synaptic transmission.

We sought to further characterize whether pharmacological restoration of GABAergic inhibition could prevent the effect of tDCS on AHN. GABA exerts its effects on AHN by acting on both ionotropic $GABA_A$ and metabotropic $GABA_B$ receptors. $GABA_A$ receptor activation has been shown to maintain NSPC quiescence and enhance neuronal maturation (Ge et al., 2006; Song et al., 2012), whereas $GABA_B$ receptor activation suppresses NSPC proliferation and neuroblast differentiation (Felice et al., 2012; Giachino et al., 2014). As our data show that multisession anodal tDCS increases NSPC proliferation, differentiation, and survival, we next investigated whether treatment of mice with the $GABA_B$ receptor positive allosteric modulator, Rac-BHFF, could reduce the effect of tDCS. For this, we pretreated mice from sham or tDCS group with Rac-BHFF 30 min before subjected to a single intraperitoneal injection of BrdU to evaluate the proliferation of NSPCs. We found that Rac-BHFF pretreatment significantly decreased numbers of $BrdU^+Ki67^+$ cells in both dorsal (Fig. 10*A*,*B*) and ventral DG (Fig. 10*A*,*C*) of tDCS mice compared with vehicle-treated tDCS group.

Discussion

Adult neurogenesis represents a remarkable form of neuroplasticity that is tightly regulated by a variety of physiological stimuli and pathologic states (Toda et al., 2019; Denoth-Lippuner and Jessberger, 2021). Two brain regions where adult neurogenesis has been best described in mammals are the subgranular zone (SGZ) of the hippocampal DG and the subventricular zone (SVZ) of the lateral ventricles. Previous studies have demonstrated that repeated tDCS effectively accelerate rehabilitation of middle cerebral artery occlusion-induced motor function deficits in rats by promoting neurogenesis in the SVZ (Braun et al., 2016; Zhang et al., 2020), but no studies have looked at the effect of tDCS on adult neurogenesis in the SGZ of the hippocampal DG in healthy animals and determine its functional impact. This study uncovers a novel role for anodal tDCS as a positive modulator of AHN in the healthy mammalian brain. Our results indicate that *in vivo* exposure of mice to multisession

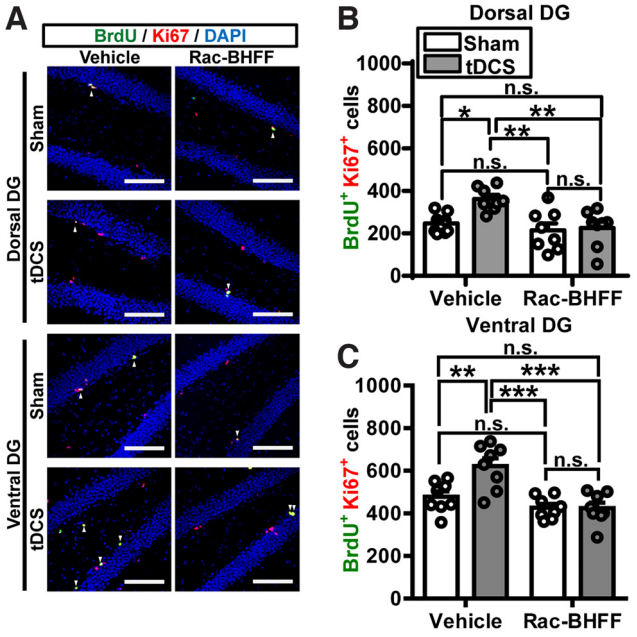

Figure 10. Pharmacological restoration of GABAergic inhibition prevents the effect of tDCS on adult hippocampal neurogenesis. ***A***, Representative immunofluorescence images of dorsal and ventral hippocampal DG sections from vehicle-treated or Rac-BHFF (30 mg/kg)-treated sham and tDCS group triple stained for BrdU (green), Ki67 (red), and DAPI (blue) 2 h after BrdU injection. The white arrowhead indicates $BrdU^+Ki67^+DAPI^+$ cells. Scale bar: 100 μm. ***B***, Quantification of the total number of $BrdU^+Ki67^+$ cells in dorsal DG of vehicle-treated or Rac-BHFF-treated sham and tDCS mice at 2 h after BrdU injection (two-way ANOVA, Group: $F_{(1,28)} = 5.93$, $p = 0.021$; Drug treatment: $F_{(1,28)} = 10.69$, $p = 0.002$; Interaction: $F_{(1,28)} = 4.03$, $p = 0.054$; $n = 8$ in each group; Bonferroni's *post hoc* multiple comparisons test, $p_{\text{vehicle + sham versus vecicle + tDCS}} = 0.0236$, $p_{\text{vehicle + tDCS versus Rac-BHFF + sham}} = 0.0023$, $p_{\text{vehicle + tDCS versus Rac-BHFF + tDCS}} = 0.0051$). ***C***, Quantification of the total number of $BrdU^+Ki67^+$ cells in ventral DG of vehicle-treated or Rac-BHFF-treated sham and tDCS mice at 2 h after BrdU injection (two way ANOVA, Group: $F_{(1,28)} = 6.73$, $p = 0.014$; Drug treatment: $F_{(1,28)} = 20.71$, $p < 0.001$; Interaction: $F_{(1,28)} = 7.07$, $p = 0.012$; $n = 8$ in each group; Bonferroni's *post hoc* multiple comparisons test, $p_{\text{vehicle + sham versus vecicle + tDCS}} = 0.0054$, $p_{\text{vehicle + tDCS versus Rac-BHFF + sham}} < 0.0001$, $p_{\text{vehicle + tDCS versus Rac-BHFF + tDCS}} < 0.0001$). Data are presented as mean ± SEM, $^*p < 0.05$, $^{**}p < 0.01$, and $^{***}p < 0.001$.

anodal tDCS increases AHN and therefore contributes to enhance context discrimination. Molecular analysis showed that this beneficial effect of tDCS is associated with reduced GABAergic inhibition in the DG.

Owing to promising clinical outcomes of tDCS in the treatment of a wide range of neurologic and psychiatric disorders, much effort has sought to identify its cellular and molecular mechanisms of action for more rational and appropriate use of this technique in clinical practices. One of the most accepted effects of tDCS is its acute ability to modify neuronal membrane polarity and hence alter resting membrane threshold for action potential generation (Stagg and Nitsche, 2011). Of particular interest, the effects of tDCS are observed not only during stimulation period but also after termination of stimulation. As a possible mechanism of action, it was hypothesized that the long-lasting after-effects of tDCS are mediated by modulating activity-dependent synaptic plasticity (Pilato et al., 2012; Cirillo et al., 2017). In support, several studies have shown that anodal tDCS applied over the hippocampus enhanced hippocampal LTP and this effect was observed for a few hours or even up to a week after stimulation (Rohan et al., 2015; Podda et al., 2016; Yu et al., 2019). Here, we extend these findings and demonstrate that multisession anodal tDCS can increase AHN. Specifically, we found that our stimulation protocol significantly increased NSPC proliferation and promoted neuronal differentiation and survival of newly generated DGCs. Consistent with an increased NSPC proliferation, we found that tDCS-treated mice exhibited increased cell cycle reentry and decreased cell cycle exit of proliferative progenitor cells. In addition, rather than a change in quiescent NSPC pool, we found that tDCS increases the numbers of all three major NSPC subtypes, suggesting that cell fate transition of NSPCs is not altered by tDCS treatment. Particularly relevant to this study is that *in vivo* repeated exposure to physical stimuli, such as extremely low-frequency electromagnetic fields (ELFEFs), has also been shown to enhance AHN by increasing NSPC proliferation, neuronal differentiation and survival (Cuccurazzu et al., 2010; Podda et al., 2014), suggesting similar mechanisms of action between tDCS and ELFEFs.

Pattern separation is a network mechanism responsible for mnemonic discrimination of similar representations in a distinct and nonoverlapping manner. It occurs in multiple brain regions, including the hippocampus, perirhinal cortex and parahippocampal gyrus (Yassa and Stark, 2011; Reagh and Yassa, 2014). Among them, the DG of the hippocampus in particular has long been postulated as a key region contributing to pattern separation because of its sparse activity pattern (Rolls, 2013; Kim et al., 2020). Since newly generated DGCs may modify the activity of the entire DG, AHN is expected to contribute to DG functions in decreasing memory inference. In agreement with previous studies showing that AHN subserves contextual fear discrimination (Clelland et al., 2009; Sahay et al., 2011), our results show that mice subjected to multisession anodal tDCS exhibited increased survival of newly generated DGCs in the adult hippocampus and enhanced performance in contextual fear discrimination. Our current results show a clear correlation between tDCS-mediated increase in AHN and enhancement in context discrimination in mice. However, we noted that this result differs from observations made in a prior human study, which reported that three sessions of bilateral tDCS over the temporal lobes decreases participants' pattern separation performance relative to sham stimulation using a mnemonic similarity task (Cappiello et al., 2016). One possible explanation is that human and rodents may use different strategies or neuronal patterns of activity to capture signals for decreasing interference between similar memories (Leal and Yassa, 2018). In addition, the different protocols of tDCS exposure (three sessions separated by 1 d vs once daily for 10 d totally) and cranial electrode placement (the anterior temporal lobes vs over the hippocampus) may also account, at least in part, for the differences in results obtained by Leal and Yassa (2018) and our own. Future studies are required to test these possibilities.

Regarding molecular mechanisms underlying tDCS-induced enhancement of AHN, our data suggest that reduced GABAergic inhibition plays a critical role. Magnetic resonance studies in humans have highlighted tDCS influences on synaptic plasticity by the modulation of excitatory and inhibitory neurotransmission. In both young and older adults, anodal tDCS has been found to induce a reduction of GABA levels in primary sensorimotor cortices (Stagg et al., 2009; Antonenko et al., 2017), an outcome known to be an important determinant of motor learning. To our knowledge, this is the first study to use electrophysiological measures to directly assess tDCS-induced alterations of GABAergic inhibitory tone in hippocampal DG of animal model. We provided evidence that multisession anodal tDCS resulted in reduced GABAergic tonic currents and the frequency of mIPSCs in the DG, indicating that multisession tDCS produce an enduring reduction in GABA release. Given the well-recognized inhibitory role of GABAergic signaling in

regulating AHN (Felice et al., 2012; Song et al., 2012; Giachino et al., 2014), the reduced GABAergic inhibitory tone may expectedly contribute to the increased AHN observed in our tDCS protocol. Since we made whole-cell recordings from randomly selected DGCs, we cannot ensure that all recorded cells were mature DGCs. Future work is warranted to explore whether the effect of tDCS on AHN results from a reduction of inhibitory influence of GABA on circuit excitation or a direct effect of GABA signaling in regulating NSPC proliferation. Consistent with our prediction, we found that pharmacological restoration of GABAergic inhibition effectively reverses tDCS-induced enhancement of NSPC proliferation. It seems counterintuitive that pharmacological activation of $GABA_B$ receptors with Rac-BHFF alone did not result in a decrease of AHN. This finding is consistent with a previous study showing that although genetic and pharmacological inhibition of $GABA_B$ receptor signaling increases proliferation of NSPCs, direct activation of $GABA_B$ receptors with baclofen does not significantly affect the number of NSPCs (Giachino et al., 2014). One interpretation of this finding is that the ability of $GABA_B$ receptors to modulate the proliferation of NSPCs is near the ceiling under normal conditions. As a result, its effect can no longer be enhanced. Interestingly, while BDNF is a critical determinant of the single session tDCS effects (Cocco et al., 2018) and BDNF in the DG has an important role in behavioral pattern separation, in particular during the consolidation of pattern-separated memories (Bekinschtein et al., 2014), it is unlikely that the observed tDCS-induced enhancement of AHN and context discrimination are resulted from a long-lasting increase BDNF levels following multisession anodal tDCS application. Indeed, we did not observe any significant changes in the expression levels of BDNF proteins in the DG 1 or 28 d after last stimulation. Therefore, future studies will have to explore whether single session and multiple sessions of anodal tDCS may use distinct mechanisms to exert their neuromodulator effects.

Our study has some limitations. First, this study only used male mice for test subjects. Therefore, additional studies are warranted to determine whether our findings can be extrapolated to female mice. Second, to more directly confirm the functional integration of newly generated DGCs into the existing hippocampal circuitry, future studies employing a combination of electrophysiology and retrovirus-mediated birth-dating and labeling may help to tackle this issue (Ge et al., 2006). Third, in a translational perspective, an important consideration is the equivalence of our stimulation protocol to those applied in humans. It is estimated that current density across the mouse brain in our experimental conditions is around three orders of magnitude greater than human tDCS (~79 vs 0.1 A/m^2 in human; Barbati et al., 2020). Further studies are needed to determine the minimal amount of current necessary in our model to elicit increased AHN and enhanced cognitive functions.

Collectively, our study provides evidence that *in vivo* multisession anodal tDCS can increase AHN and that this effect is associated with enhanced context discrimination. These effects correlate with reduced GABAergic inhibition in the DG of the hippocampus. These findings extend our knowledge of the cellular and molecular mechanisms involved in the after-effects of tDCS, and underscore the probable utility of tDCS for improving cognitive decline associated with normal aging and neurodegenerative disorders.

References

Alizadehgoradel J, Nejati V, Sadeghi Movahed F, Imani S, Taherifard M, Mosayebi-Samani M, Vicario CM, Nitsche MA, Salehinejad MA (2020) Repeated stimulation of the dorsolateral-prefrontal cortex improves executive dysfunctions and craving in drug addiction: a randomized, double-blind, parallel-group study. Brain Stimul 13:582–593.

Antonenko D, Schubert F, Bohm F, Ittermann B, Aydin S, Hayek D, Grittner U, Flöel A (2017) tDCS-induced modulation of GABA levels and resting-state functional connectivity in older adults. J Neurosci 37:4065–4073.

Antonenko D, Hayek D, Netzband J, Grittner U, Flöel A (2019) tDCS-induced episodic memory enhancement and its association with functional network coupling in older adults. Sci Rep 9:2273.

Barbati SA, Cocco S, Longo V, Spinelli M, Gironi K, Mattera A, Paciello F, Colussi C, Podda MV, Grassi C (2020) Enhancing plasticity mechanisms in the mouse motor cortex by anodal transcranial direct-current stimulation: the contribution of nitric oxide signaling. Cereb Cortex 30:2972–2985.

Bekinschtein P, Cammarota M, Medina JH (2014) BDNF and memory processing. Neuropharmacology 76:677–683.

Braun R, Klein R, Walter HL, Ohren M, Freudenmacher L, Getachew K, Ladwig A, Luelling J, Neumaier B, Endepols H, Graf R, Hoehn M, Fink GR, Schroeter M, Rueger MA (2016) Transcranial direct current stimulation accelerates recovery of function, induces neurogenesis and recruits oligodendrocyte precursors in a rat model of stroke. Exp Neurol 279:127–136.

Brunoni AR, Nitsche MA, Bolognini N, Bikson M, Wagner T, Merabet L, Edwards DJ, Valero-Cabre A, Rotenberg A, Pascual-Leone A, Ferrucci R, Priori A, Boggio PS, Fregni F (2012) Clinical research with transcranial direct current stimulation (tDCS): challenges and future directions. Brain Stimul 5:175–195.

Cappiello M, Xie W, David A, Bikson M, Zhang W (2016) Transcranial direct current stimulation modulates pattern separation. Neuroreport 27:826–832.

Chan MMY, Yau SSY, Han YMY (2021) The neurobiology of prefrontal transcranial direct current stimulation (tDCS) in promoting brain plasticity: a systematic review and meta-analyses of human and rodent studies. Neurosci Biobehav Rev 125:392–416.

Chenn A, Walsh CA (2002) Regulation of cerebral cortical size by control of cell cycle exit in neural precursors. Science 297:365–369.

Choi SH, Bylykbashi E, Chatila ZK, Lee SW, Pulli B, Clemenson GD, Kim E, Rompala A, Oram MK, Asselin C, Aronson J, Zhang C, Miller SJ, Lesinski A, Chen JW, Kim DY, van Praag H, Spiegelman BM, Gage FH, Tanzi RE (2018) Combined adult neurogenesis and BDNF mimic exercise effects on cognition in an Alzheimer's mouse model. Science 361:eaan8821.

Christian KM, Song H, Ming GL (2014) Functions and dysfunctions of adult hippocampal neurogenesis. Annu Rev Neurosci 37:243–262.

Cirillo G, Di Pino G, Capone F, Ranieri F, Florio L, Todisco V, Tedeschi G, Funke K, Di Lazzaro V (2017) Neurobiological after-effects of non-invasive brain stimulation. Brain Stimul 10:1–18.

Clelland CD, Choi M, Romberg C, Clemenson GD Jr, Fragniere A, Tyers P, Jessberger S, Saksida LM, Barker RA, Gage FH, Bussey TJ (2009) A functional role for adult hippocampal neurogenesis in spatial pattern separation. Science 325:210–213.

Cocco S, Podda MV, Grassi C (2018) Role of BDNF signaling in memory enhancement induced by transcranial direct current stimulation. Front Neurosci 12:427.

Cuccurazzu B, Leone L, Podda MV, Piacentini R, Riccardi E, Ripoli C, Azzena GB, Grassi C (2010) Exposure to extremely low-frequency (50 Hz) electromagnetic fields enhances adult hippocampal neurogenesis in C57BL/6 mice. Exp Neurol 226:173–182.

Denoth-Lippuner A, Jessberger S (2021) Formation and integration of new neurons in the adult hippocampus. Nat Rev Neurosci 22:223–236.

Engin E, Zarnowska ED, Benke D, Tsvetkov E, Sigal M, Keist R, Bolshakov VY, Pearce RA, Rudolph U (2015) Tonic inhibitory control of dentate gyrus granule cells by α5-containing GABAA receptors reduces memory interference. J Neurosci 35:13698–13712.

Farahani F, Kronberg G, FallahRad M, Oviedo HV, Parra LC (2021) Effects of direct current stimulation on synaptic plasticity in a single neuron. Brain Stimul 14:588–597.

Felice D, O'Leary OF, Pizzo RC, Cryan JF (2012) Blockade of the GABAB receptor increases neurogenesis in the ventral but not dorsal adult

hippocampus: relevance to antidepressant action. Neuropharmacology 63:1380–1388.
Ferrucci R, Mameli F, Guidi I, Mrakic-Sposta S, Vergari M, Marceglia S, Cogiamanian F, Barbieri S, Scarpini E, Priori A (2008) Transcranial direct current stimulation improves recognition memory in Alzheimer disease. Neurology 71:493–498.
Flöel A (2014) tDCS-enhanced motor and cognitive function in neurological diseases. Neuroimage 85:934–947.
Fregni F, Boggio PS, Nitsche M, Bermpohl F, Antal A, Feredoes E, Marcolin MA, Rigonatti SP, Silva MT, Paulus W, Pascual-Leone A (2005) Anodal transcranial direct current stimulation of prefrontal cortex enhances working memory. Exp Brain Res 166:23–30.
Fregni F, Boggio PS, Santos MC, Lima M, Vieira AL, Rigonatti SP, Silva MT, Barbosa ER, Nitsche MA, Pascual-Leone A (2006) Noninvasive cortical stimulation with transcranial direct current stimulation in Parkinson's disease. Mov Disord 21:1693–1702.
Garthe A, Behr J, Kempermann G (2009) Adult-generated hippocampal neurons allow the flexible use of spatially precise learning strategies. PLoS One 4:e5464.
Ge S, Goh EL, Sailor KA, Kitabatake Y, Ming GL, Song H (2006) GABA regulates synaptic integration of newly generated neurons in the adult brain. Nature 439:589–593.
Giachino C, Barz M, Tchorz JS, Tome M, Gassmann M, Bischofberger J, Bettler B, Taylor V (2014) GABA suppresses neurogenesis in the adult hippocampus through $GABA_B$ receptors. Development 141:83–90.
Göder R, Baier PC, Beith B, Baecker C, Seeck-Hirschner M, Junghanns K, Marshall L (2013) Effects of transcranial direct current stimulation during sleep on memory performance in patients with schizophrenia. Schizophr Res 144:153–154.
Jones BW, Deem J, Younts TJ, Weisenhaus M, Sanford CA, Slack MC, Chin J, Nachmanson D, McKennon A, Castillo PE, McKnight GS (2016) Targeted deletion of AKAP7 in dentate granule cells impairs spatial discrimination. Elife 5:e20695.
Kempermann G, Song H, Gage FH (2015) Neurogenesis in the adult hippocampus. Cold Spring Harb Perspect Biol 7:a018812.
Kim KR, Lee SY, Yoon SH, Kim Y, Jeong HJ, Lee S, Suh YH, Kang JS, Cho H, Lee SH, Kim MH, Ho WK (2020) Kv4.1, a key ion channel for low frequency firing of dentate granule cells, is crucial for pattern separation. J Neurosci 40:2200–2214.
Leal SL, Yassa MA (2018) Integrating new findings and examining clinical applications of pattern separation. Nat Neurosci 21:163–173.
Lin YT, Chen CC, Huang CC, Nishimori K, Hsu KS (2017) Oxytocin stimulates hippocampal neurogenesis via oxytocin receptor expressed in CA3 pyramidal neurons. Nat Commun 8:537.
Lugert S, Basak O, Knuckles P, Haussler U, Fabel K, Götz M, Haas CA, Kempermann G, Taylor V, Giachino C (2010) Quiescent and active hippocampal neural stem cells with distinct morphologies respond selectively to physiological and pathological stimuli and aging. Cell Stem Cell 6:445–456.
Malherbe P, Masciadri R, Norcross RD, Knoflach F, Kratzeisen C, Zenner MT, Kolb Y, Marcuz A, Huwyler J, Nakagawa T, Porter RH, Thomas AW, Wettstein JG, Sleight AJ, Spooren W, Prinssen EP (2008) Characterization of (R,S)-5,7-di-tert-butyl-3-hydroxy-3-trifluoromethyl-3H-benzofuran-2-one as a positive allosteric modulator of $GABA_B$ receptors. Br J Pharmacol 154:797–811.
Miller SM, Sahay A (2019) Functions of adult-born neurons in hippocampal memory interference and indexing. Nat Neurosci 22:1565–1575.
Niibori Y, Yu TS, Epp JR, Akers KG, Josselyn SA, Frankland PW (2012) Suppression of adult neurogenesis impairs population coding of similar contexts in hippocampal CA3 region. Nat Commun 3:1253.
Pilato F, Profice P, Ranieri F, Capone F, Di Iorio R, Florio L, Di Lazzaro V (2012) Synaptic plasticity in neurodegenerative diseases evaluated and modulated by in vivo neurophysiological techniques. Mol Neurobiol 46:563–571.
Pedron S, Monnin J, Haffen E, Sechter D, Van Waes V (2014) Repeated transcranial direct current stimulation prevents abnormal behaviors associated with abstinence from chronic nicotine consumption. Neuropsychopharmacology 39:981–988.
Pelletier SJ, Cicchetti F (2014) Cellular and molecular mechanisms of action of transcranial direct current stimulation: evidence from in vitro and in vivo models. Int J Neuropsychopharmacol 18:pyu047.
Pikhovych A, Stolberg NP, Jessica Flitsch L, Walter HL, Graf R, Fink GR, Schroeter M, Rueger MA (2016) Transcranial direct current stimulation modulates neurogenesis and microglia activation in the mouse brain. Stem Cells Int 2016:2715196.
Podda MV, Leone L, Barbati SA, Mastrodonato A, Li Puma DD, Piacentini R, Grassi C (2014) Extremely low-frequency electromagnetic fields enhance the survival of newborn neurons in the mouse hippocampus. Eur J Neurosci 39:893–903.
Podda MV, Cocco S, Mastrodonato A, Fusco S, Leone L, Barbati SA, Colussi C, Ripoli C, Grassi C (2016) Anodal transcranial direct current stimulation boosts synaptic plasticity and memory in mice via epigenetic regulation of Bdnf expression. Sci Rep 6:22180.
Reagh ZM, Yassa MA (2014) Object and spatial mnemonic interference differentially engage lateral and medial entorhinal cortex in humans. Proc Natl Acad Sci U S A 111:E4264–4273.
Reis J, Schambra HM, Cohen LG, Buch ER, Fritsch B, Zarahn E, Celnik PA, Krakauer JW (2009) Noninvasive cortical stimulation enhances motor skill acquisition over multiple days through an effect on consolidation. Proc Natl Acad Sci U S A 106:1590–1595.
Rohan JG, Carhuatanta KA, McInturf SM, Miklasevich MK, Jankord R (2015) Modulating hippocampal plasticity with in vivo brain stimulation. J Neurosci 35:12824–12832.
Rolls ET (2013) The mechanisms for pattern completion and pattern separation in the hippocampus. Front Syst Neurosci 7:74.
Sahay A, Wilson DA, Hen R (2011) Pattern separation: a common function for new neurons in hippocampus and olfactory bulb. Neuron 70:582–588.
Salic A, Mitchison TJ (2008) A chemical method for fast and sensitive detection of DNA synthesis in vivo. Proc Natl Acad Sci U S A 105:2415–2420.
Sibbe M, Kulik A (2017) GABAergic regulation of adult hippocampal neurogenesis. Mol Neurobiol 54:5497–5510.
Song J, Zhong C, Bonaguidi MA, Sun GJ, Hsu D, Gu Y, Meletis K, Huang ZJ, Ge S, Enikolopov G, Deisseroth K, Luscher B, Christian KM, Ming GL, Song H (2012) Neuronal circuitry mechanism regulating adult quiescent neural stem-cell fate decision. Nature 489:150–154.
Stagg CJ, Nitsche MA (2011) Physiological basis of transcranial direct current stimulation. Neuroscientist 17:37–53.
Stagg CJ, Best JG, Stephenson MC, O'Shea J, Wylezinska M, Kincses ZT, Morris PG, Matthews PM, Johansen-Berg H (2009) Polarity-sensitive modulation of cortical neurotransmitters by transcranial stimulation. J Neurosci 29:5202–5206.
Stone SS, Teixeira CM, Devito LM, Zaslavsky K, Josselyn SA, Lozano AM, Frankland PW (2011) Stimulation of entorhinal cortex promotes adult neurogenesis and facilitates spatial memory. J Neurosci 31:13469–13484.
Suh H, Consiglio A, Ray J, Sawai T, D'Amour KA, Gage FH (2007) In vivo fate analysis reveals the multipotent and self-renewal capacities of $Sox2^+$ neural stem cells in the adult hippocampus. Cell Stem Cell 1:515–528.
Toda T, Parylak SL, Linker SB, Gage FH (2019) The role of adult hippocampal neurogenesis in brain health and disease. Mol Psychiatry 24:67–87.
Wu YJ, Tseng P, Chang CF, Pai MC, Hsu KS, Lin CC, Juan CH (2014) Modulating the interference effect on spatial working memory by applying transcranial direct current stimulation over the right dorsolateral prefrontal cortex. Brain Cogn 91:87–94.
Wu YJ, Lin CC, Yeh CM, Chien ME, Tsao MC, Tseng P, Huang CW, Hsu KS (2017) Repeated transcranial direct current stimulation improves cognitive dysfunction and synaptic plasticity deficit in the prefrontal cortex of streptozotocin-induced diabetic rats. Brain Stimul 10:1079–1087.
Yassa MA, Stark CE (2011) Pattern separation in the hippocampus. Trends Neurosci 34:515–525.
Yu TH, Wu YJ, Chien ME, Hsu KS (2019) Transcranial direct current stimulation induces hippocampal metaplasticity mediated by brain-derived neurotrophic factor. Neuropharmacology 144:358–367.
Zhang KY, Rui G, Zhang JP, Guo L, An GZ, Lin JJ, He W, Ding GR (2020) Cathodal tDCS exerts neuroprotective effect in rat brain after acute ischemic stroke. BMC Neurosci 21:21.